Microelectronic Engineering 153 (2016) 132–136

Contents lists available at ScienceDirect

Microelectronic Engineering

journal homepage: www.elsevier.com/locate/mee

Research paper

Fabrication of high-aspect ratio GaN nanostructures for advanced photonic devices

E.D. Le Boulbar [a,*], C.J. Lewins [a], D.W.E. Allsopp [a], C.R. Bowen [b], P.A. Shields [a]

[a] Department of Electronic and Electrical Engineering, University of Bath, BA2 7AY, UK
[b] Department of Mechanical Engineering, University of Bath, BA2 7AY, UK

ARTICLE INFO

Article history:
Received 6 November 2015
Received in revised form 15 March 2016
Accepted 27 March 2016
Available online 06 April 2016

Keywords:
GaN
Plasma etching
Photonic
Nanorod
Nanopore
Core-shell

ABSTRACT

High-aspect-ratio GaN-based nanostructures are of interest for advanced photonic crystal and core-shell devices. Nanostructures grown by a bottom-up approach are limited in terms of doping, geometry and shape which narrow their potential application areas. In contrast, high uniformity and a greater diversity of shape and design can be produced via a top-down etching approach. However, a detailed understanding of the role of etch process parameters is lacking for creating high-aspect ratio nanorods and nanopores. Here we report a systematic analysis on the role of temperature and pressure on the fabrication of nanorod and nanopore arrays in GaN. Our results show a threshold in the etch behaviour at a temperature of ~125 °C, which greatly enhances the verticality of the GaN nanorods, whilst the modification of the pressure enables a fine tuning of the nanorod profile. For nanopores we show that the use of higher temperatures at higher pressures enables the fabrication of nanopores with an undercut profile. Such a profile is important for controlling the optical field in photonic crystal-based devices. Therefore we expect the ability to create such nanostructures to form the foundation for new advanced LED designs.

1. Introduction

III-Nitride high-aspect ratio nanostructures such as arrays of ordered nanorods and nanopores, for which the lateral dimensions of pillars and holes, respectively, are submicron and the aspect ratio is greater than one, are of great interest for the next generation of devices such as core-shell light emitting diodes [1–3], non-linear photonic diodes [4], photonic crystal emitters [5–7] and sensors [8–11]. It has been reported that the optical emission properties of InGaN/GaN nanorod arrays, such as the directivity or the enhancement of photonic crystal features, strongly depends on the shape, diameter, height and density of the nanorod arrays [6,7,12]. The use of nanopore arrays to create photonic crystals within suspended membranes also depends on the losses induced by scattering induced by the fabrication process [13,14]. Therefore, the ability to accurately control the nanorod and nanopore parameters is essential for device fabrication.

The use of deep-ultraviolet or nanoimprint lithography (NIL) to create nanoscale metal mask, combined with dry-etching, allows the creation of arrays of nanorods and nanopores on a wafer-scale through top-down processing [15,16]. The nanostructure diameter, dimension and geometry of the array can be controlled by carefully designing the stamp, whilst the height and shape of the nanostructures can be tuned by controlling the parameters of the dry-etching process [16]. The nanorod profile plays an important role in whether photonic crystal effects are observed in InGaN/GaN nanorods. The introduction of an undercut profile creates a strong index guiding which supports the formation of Bloch modes [6], allowing the light to be guided in-plane and causing the existence of a photonic band gap.

The use of an epitaxial regrowth step after the etching of the nanostructure by Metal Organic Vapour Phase Epitaxy (MOVPE) can also be implemented to reduce etch damage induced by the top-down process [17]. Furthermore, it can be used to create an active region, such as an InGaN quantum well, for the fabrication of InGaN/GaN radial core shell structures for LEDs [17–19] or sensors [8–10].

In our previous study, we found the temperature during plasma etching had a critical effect on the sidewall verticality of high-aspect-ratio GaN nanorods [20]. In this article, we examine more deeply the impact of temperature and pressure on the shape of the GaN nanorods and nanopores using Cl_2/Ar chemistry. This chemistry was chosen for its simplicity and because it produces controllable etch rates [21]. Using an etch temperature greater than 125 °C has been found to enable the formation of high-aspect-ratio nanorods with a vertical profile, and both the pressure and temperature are critical parameters for the fabrication of undercut nanorods and nanopores.

2. Experimental

A nanoimprint-lithography-based lift-off technique was used to create regular hexagonal arrays of metal dots or holes for use as a hard mask for nanorods and nanopores respectively [15]. The nanoimprint

* Corresponding author.
E-mail address: E.Le.Boulbar@bath.ac.uk (E.D. Le Boulbar).

http://dx.doi.org/10.1016/j.mee.2016.03.058

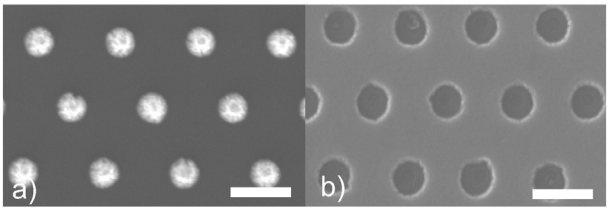

Fig. 1. SEM planar view images of the nickel metal mask created by NIL and lift-off according to Ref. [15] a) nanodot and b) nanohole arrays. Scale bars represent 500 nm.

masters comprised either 230 nm features on a 600 nm pitch or 600 nm features on a 2 μm pitch. Fig. 1 shows an example of the nanoscale metal mask used for GaN etching with a pitch of 600 nm. The size of the metal dots in Fig. 1a was measured to be approximately 280 nm whilst the size of the holes in the metal mask in Fig. 1b was approximately 250 nm.

Conventional MOVPE-grown, Ga-polar, c-plane, silicon-doped GaN-on-sapphire templates of thickness approximately 5 μm were used for creating both GaN nanorods and nanopores in an ICP dry etch system (Oxford Instruments System 100 Cobra). A mixed Cl_2/Ar gas composition with a 5:1 ratio was used for the GaN etching. This composition represents a good compromise between a fast GaN etching rate and reduced mask erosion, both of which are important for obtaining high-aspect-ratio structures. The following dry etching parameters for nanorod and nanopore etching were kept constant: Cl_2 flow 50 sccm, Ar flow 10 sccm, RIE power 120 W, ICP source power 800 W. The pressure was varied between 9 mTorr and 15 mTorr, and the temperature was varied between 75 °C to 175 °C for nanorods, and 150 °C to 350 °C for nanopores. Higher temperatures were studied for the nanopores in order to determine whether the etch limitations, to be discussed later, could be overcome. The effect of etch duration was investigated from 5 to 30 min at the different pressures and temperatures for both structures. The temperature of the bottom electrode, on which the sample was placed, was controlled and measured in-situ. The variation of measured temperature never exceeded the set temperature by more than 5 °C during the overall etching process. In order to minimize additional plasma heating of the sample, a pause of one minute was introduced after each minute of etching. Secondary electron images were taken from the centre of the sample with a Hitachi S-4300 Scanning Electron Microscope (SEM) after cleaving it in half. The height and diameter of the nanostructure were extracted from the SEM image. Measurements were taken on more than five nanostructures to obtain representative and accurate dimensions.

3. Results and discussion

Fig. 2 shows SEM cross sectional images of GaN nanorods etched for 10 min at 9 mTorr for various temperatures. The increase of temperature from 75 °C to 175 °C has three effects on the nanorod characteristics: 1) an increase of the etch depth, 2) a decrease in the nanorod diameter, and 3) a modification of the nanorod sidewall angle from a tapered to a vertical profile.

Fig. 3 summarises the nanorod etching characteristics: the etch rate, rod diameter, and sidewall angle as measured from SEM images, as a function of temperature.

A noticeable step change in the etch rate, from 340 nm.min^{-1} to 375 nm.min^{-1}, is observed for temperatures below and above a critical temperature between 100 and 125 °C (Fig. 3a). In addition, a clear discontinuity is observed in the nanorod diameter temperature dependence at 125 °C (Fig. 3b, diameter measured at half the nanorod height). The decrease of diameter with temperature is much greater below this critical value than above it, dropping from 2.3 nm.°C^{1} to 0.2 nm.°C^{-1}. Furthermore the rise of temperature from 75 °C to 100 °C improves the verticality of the nanorods, with a decrease of the sidewall angle from 10° to 0.4° for this set of etching parameters

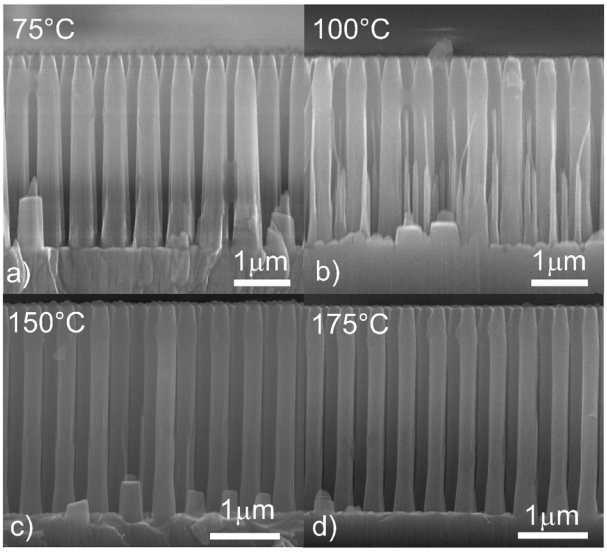

Fig. 2. SEM cross-sectional images of GaN nanorod arrays etched at different temperatures using 800 W ICP, 120 W RIE, 9 mTorr, Cl_2/Ar flows: 50/10 sccm.

(Fig. 3c). A further increase of temperature to 175 °C leads to a very small undercut (Inset Fig. 3c).

The modification of the etch rate and the nanorod diameter discontinuity, both observed around 100–125 °C, suggest a change in the etching mechanism. The sloped sidewall of 10° found at 75 °C indicates a

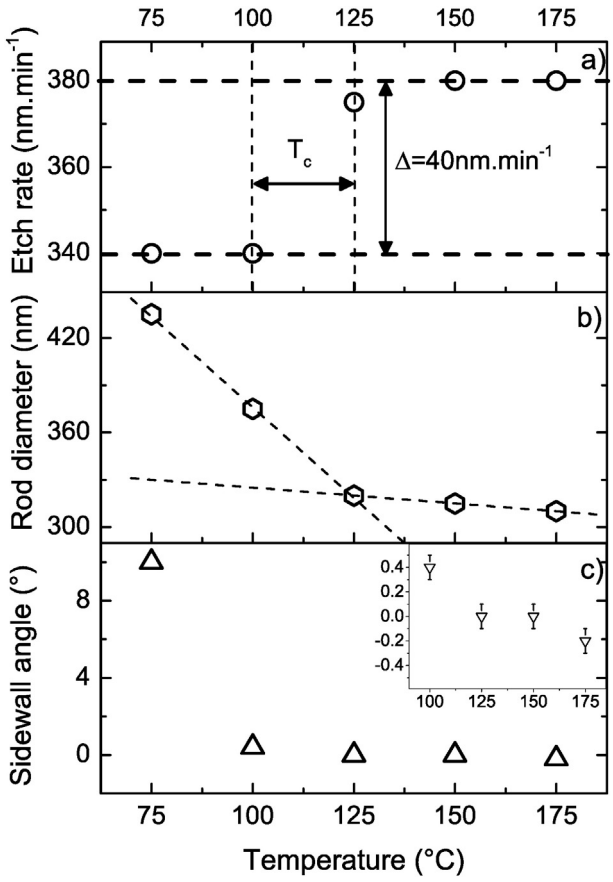

Fig. 3. Etch rate, rod diameter and sidewall angle of GaN nanorods measured from cross-sectional SEM images after etching using 800 W ICP, 120 W RIE, 9 mTorr, Cl_2/Ar 50/10 sccm from 75 °C to 175 °C for 10 min. The inset shows the sidewall angle profile from 100 °C to 175 °C.

sputter-dominated regime with limited volatility of etch by-products. The importance of the volatility of the etched by-products is confirmed by the reduction of sidewall angle from 10° to 0.4° at 100 °C as well as the decrease of nanorod diameter from 100 °C to 125 °C.

In general there are two main effects influencing the sidewall profile during dry etching. The first is the angle of incidence of the etching ions, while the second is the formation, during the etching process, of a protective layer resistant to the chemical component of the plasma etching. Once this layer has been formed, further chemical etching of the GaN can continue only once this protective layer has been removed. Control of the generation and removal rates of the protective layer determines the sidewall profile angle. Sputter etching in an ICP system is highly anisotropic due to two effects: firstly, the small angular distribution of incident ions leads to greater ion irradiance for the parts of the wafer where the surface is normal to the accelerating electric field than on those parts that are inclined. Secondly the sputter etch process is much less efficient for ions incident at glancing angles. For the case of GaN in Cl plasmas, it is expected that the chemical etch process involves the conversion of GaN to $(GaCl_3)_2$ or $(GaCl_3)$, thus requiring multiple collisions [22]. As the collision probability reduces for more glancing angles, the probability of etching material on the nanorod sidewall is strongly reduced. It is expected that for the GaN nanorods the formation and removal of the protective $(GaCl_3)_2$ created on the sidewalls at a particular temperature will determine the profile. The discontinuity at ~125 °C found in the etching rate and the rod diameter with temperature, indicates the point at which the protective layer is removed as fast as it is generated. The small linear decrease observed from 125 °C to 175 °C would then solely correspond to the generation rate of the protective layer on the sidewall. These temperatures are consistent with the increase of volatility of the $(GaCl_3)_2$ and $(GaCl_3)$ etch by-products around 80–150 °C [20].

Fig. 4 shows the effect of pressure on the profile of etched nanorod arrays for 600 nm features on a 2 μm pitch. The set of etch parameters used were the same as described above but the temperature and etching time were fixed as 150 °C and 12 min, respectively, whilst the pressure was varied from 10 mTorr to 15 mTorr.

Fig. 4 shows that the etching depth was reduced from 4.3 μm, 3.4 μm to 3.2 μm as the pressure increased from 10 mTorr, 12 mTorr to 15 mTorr, respectively. At 10 mTorr, nanorods with 550 nm diameter were obtained. Whilst the sidewalls are predominantly vertical, the topmost region (about 800 nm) shows a slight outward tapering. This most likely arises due to mask erosion occurring during the etching process. The increase of pressure to 12 mTorr results in the top region being less tapered since the higher pressure reduces the sputter component of the etch process, thus reducing the mask erosion and its consequences. In contrast to 10 mTorr the lower regions of the nanorod etched at 12 mTorr were also slightly undercut, with the diameter decreasing from 570 nm near the top to a minimum value of 530 nm nearer the base. A further increase of pressure to 15 mTorr led to a more pronounced undercut profile, with a linear reduction of the size of the nanorod diameter from 600 nm at the top to 270 nm at the base. The measured DC bias increased from 410 V for 10 mTorr, to 420 V for 12 mTorr, up to 440 V for 15 mTorr.

These results show the impact of the pressure on the etch mechanism, from a sputter-based process at lower pressure, predominantly due to a higher mean free path of the species, which erodes faster the hard mask, to a less anisotropic process with enhanced lateral etching at higher pressure, likely to be due to a higher scattering and a higher concentration of the species, which produced an undercut at the base of the nanorod.

The same investigation has been pursued to achieve high-aspect-ratio nanopores using an initial hole aperture diameter of 250 nm. The etching of nanopores is known to be more difficult due to the shadowing effect of neutral species and electrostatic deflection of incoming ions in the holes [23] and the greater difficulty in removing the etch by-products from the more confined nanopores.

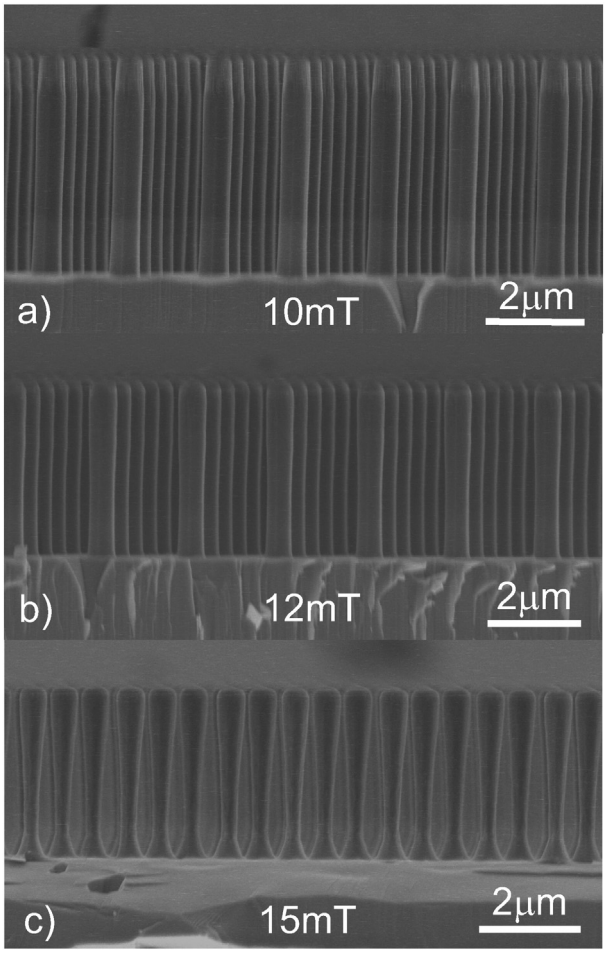

Fig. 4. SEM cross-sectional images of GaN nanorod arrays etched at different pressures at a fixed temperature of 150 °C using 800 W ICP, 120 W RIE, 9 mTorr, Cl_2/Ar flows: 50/10 sccm.

Fig. 5 shows cross-sectional SEM images of nanopore arrays after cleaving. Note that the cleave line does not necessarily pass through the centres of the nanopores, thus making the images harder to interpret than for the cleaved nanorod arrays. The nanopores were etched for 5 min at different temperatures at a fixed pressure of 15 mTorr. At 200 °C, an etch depth of 1.2 μm was achieved. However, the holes were highly tapered so that the etch depth was self-limiting. A further increase of temperature, up to 250 °C and 350 °C, helped to increase the etch depth to 1.5 μm and 1.6 μm respectively. The most noticeable feature for the higher temperatures was the large increase in the pore diameter around 550–600 nm below the mask, increasing to 350 and 380 nm for 250 °C and 350 °C, respectively. Furthermore the nanopores were wider with a flat, smooth base with a diameter of 240–250 nm, equivalent to the pore opening.

Substantial roughness within the nanopores can be seen in high resolution SEM images at 200 °C (not shown) that appears to decrease at 250 °C and has disappeared at 350 °C. At the higher temperatures the roughness is replaced by well-defined crystallographic facets (Fig. 5b and c). The presence of these facets, obtained at high temperature and pressure, implies the dominance of chemical etching in the process. Moving from 200 °C to 250 °C and above, the etching of Ga-based material is facilitated by the larger probability of forming $(GaCl_3)$ over $(GaCl_3)_2$. We believe the widening of the pores at 550–600 nm below the surface is most probably due to the deflection of incoming ions by the slightly tapered etch mask towards the nanopores sidewalls and from surface charges that deflect ions into parabolic trajectories directed towards the

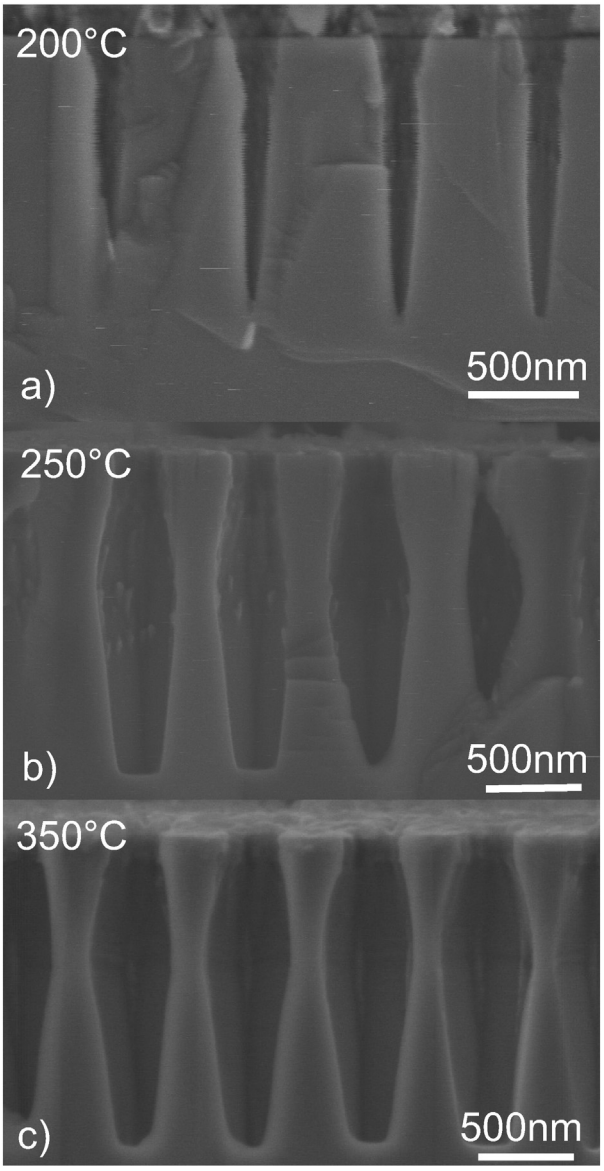

Fig. 5. SEM cross-sectional images of GaN nanopores etched for 5 min at various temperatures using 800 W ICP, 120 W RIE, 15 mTorr, Cl_2/Ar flow: 50/10 sccm.

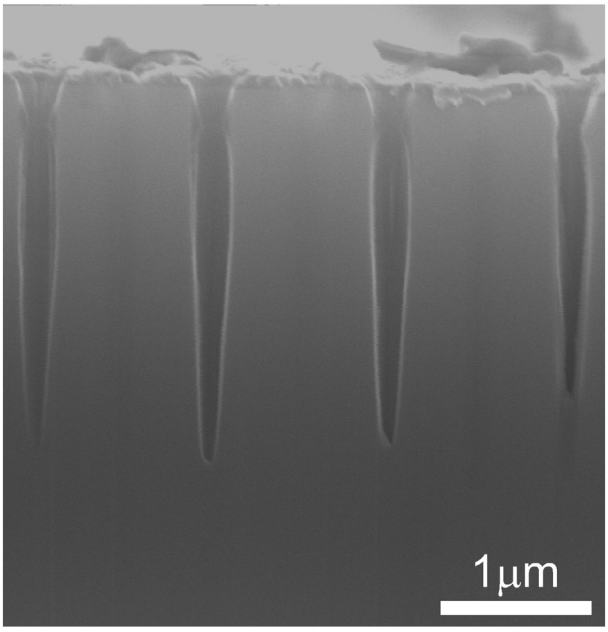

Fig. 6. SEM cross-sectional images of GaN nanopores etched for 30 min at 15 mTorr and 150 °C using 800 W ICP, 120 W RIE, Cl_2/Ar flow: 50/10 sccm.

sidewalls of the nanopores [24,25]. This leads to the pore widening at a fixed distance below the mask, independent of temperature.

Fig. 6 shows an SEM cross-sectional image of GaN nanopores etched for the much longer duration of 30 min at 15 mTorr for a temperature of 150 °C. Uniform etching was found all over the sample with an etch depth of 2.4 μm. It was found that increasing the temperature up to 250 °C did not further increase the overall aspect ratio of the nanopores. For deep-etched nanopores, whilst the tapering of the upper region varied depending on the etch parameters, the lower region of the pores was found to be tapered in all cases.

Fig. 7 shows the effect of etch duration on the aspect ratio of the nanopores. It is clearly non-linear, reaching a maximum aspect ratio of approximately 8 after 20 min. This effect is well established and known as Aspect Ratio Dependent Etching (ARDE). There are a number of factors that could have contributed to this phenomenon:

1) The etching by-products can deposit on the surface and control the evolution of the sidewall profile. The balance between simultaneous etching and formation of the passivation layer determines the overall profile during the plasma etching process. For any tapered profiles, there is a limit to the etch depth that can be achieved simply due to the geometry of the taper. For nanorods, the sidewall profile depends strongly on temperature, as shown in Fig. 3. On the other hand, nanopores were etched at temperatures up to 350 °C, without improvement in the maximum aspect ratio.
2) Depletion of the etching species within the nanopores can occur as a result of in-diffusion being impeded by reaction by-products unable to escape the evolving nanostructure or by a concentration gradient of the etching species caused by the reaction with the sidewall or geometrical shadowing of its lower regions, leading to a reduction in sidewall etching with increasing depth. Any tapering resulting from this effect will lead to a self-limiting etch depth as described above.
3) Charging of the GaN surface during the etching of high-aspect-ratio features can build up an electric field on the surface that distorts

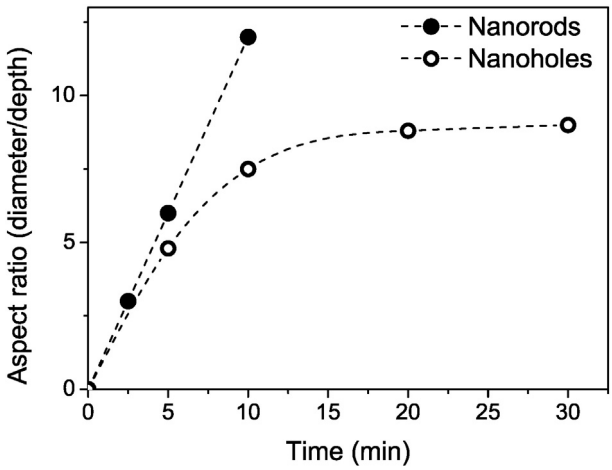

Fig. 7. Aspect ratio as a function of time for both nanorods (150 °C & 9 mTorr) and nanopores (150 °C & 15 mTorr). An aspect ratio dependent etching is found for the nanopore geometry.

the ion trajectories and prevents the charged etching species from reaching the lower regions or the nanopores.

The combination of these effects result in a reduction of the etch rate with depth leading to a non-linear etch rate with time. A comparison of the aspect ratio versus duration for nanorods and nanopores is also shown in Fig. 7. Whilst a strong non-linearity was observed for nanopores, a linear increase of the etching depth was observed for the nanorods. The contrast is striking, and is likely to result from the 'open' nature of the nanorod topology with interconnected space in-between that facilitate the transport of the neutral species and the removal of the etch by-products. This contrasts with the 'closed' nature of the nanopores in which the by-products can only be removed via the limited nanopore opening.

Potential fundamental limitations to the aspect ratio achievable for both nanorods and nanopores include: the selectivity of the metal mask, undercutting leading to eventual fracture of the template, and ARDE. For nanorods, the use of a metal mask and the increase of temperature, as well as a fine tuning of the pressure allowed us to increase the aspect ratio to greater than 12. However, in the case of nanopores, the aspect ratio is more limited.

4. Summary and conclusion

In summary, high-aspect-ratio etched nanostructures have been fabricated and their properties controlled by careful control of the ICP etching parameters. We have identified and described the effect of temperature and pressure on the etching mechanisms of GaN. The temperature has been found to dramatically enhance both sidewall verticality and the achievable etch depth, with a temperature of ~125 °C delineating two etching regimes. The pressure is also found to have an important impact on the sidewall verticality so that the sidewall profile within a nanorod array can be tuned from tapered to vertical. Furthermore higher pressure affects the mask erosion and hence the selectivity of the etch process.

In conclusion, the key parameters of temperature and pressure should be carefully controlled to design and tune nanorod profiles, both in close-packed and sparser nanorod arrays. This work provides guidelines to tune the height, diameter and profile of nanorods and nanopores which are useful for the fabrication of advanced photonic crystal devices.

Acknowledgements

Financial support is acknowledged from the EPSRC, UK via Grant No. EP/I012591/1 "Lighting the Future" and Grant No. EP/M015181/1, "Manufacturing nano-GaN". Bowen acknowledges European Union's Seventh Framework Programme (FP/2007-2013)/ERC Grant Agreement no. 320963 on Novel Energy Materials, Engineering Science and Integrated Systems (NEMESIS). The data associated with this research are available at http://doi.org/10.15125/BATH-00154 or from the corresponding author.

References

[1] N.A. Fichtenbaum, C.J. Neufeld, C. Schaake, Y. Wu, M.H. Wong, M. Grundmann, S. Keller, S.P. DenBaars, J.S. Speck, U.K. Mishra, Metalorganic chemical vapor Deposition regrowth of InGaN and GaN on N-polar pillar and stripe nanostructures, Jpn. J. Appl. Phys. 46 (2007) L230–L233, http://dx.doi.org/10.1143/JJAP.46.L230.

[2] S. Li, X. Wang, S. Fündling, M. Erenburg, J. Ledig, J. Wei, H.H. Wehmann, A. Waag, W. Bergbauer, M. Mandl, M. Strassburg, A. Trampert, U. Jahn, H. Riechert, H. Jönen, A. Hangleiter, Nitrogen-polar core-shell GaN light-emitting diodes grown by selective area metalorganic vapor phase epitaxy, Appl. Phys. Lett. 101 (2012) 032103, http://dx.doi.org/10.1063/1.4737395.

[3] S. Li, X. Wang, M.S. Mohajerani, S. Fündling, M. Erenburg, J. Wei, H.H. Wehmann, A. Waag, M. Mandl, W. Bergbauer, M. Strassburg, Dependence of N-polar GaN rod morphology on growth parameters during selective area growth by MOVPE, J. Cryst. Growth 364 (2012) 149–154, http://dx.doi.org/10.1016/j.jcrysgro.2012.11.027.

[4] S. Ko, S. Gong, Y. Cho, Nonlinear photonic diode behavior in energy-graded core − shell quantum well semiconductor rod, Nano Lett. 14 (2014) 4937–4942, http://dx.doi.org/10.1021/nl5007905.

[5] P.A. Shields, M.D.B. Charlton, C.J. Lewins, X. Gao, D.W.E. Allsopp, W.N. Wang, B. Humphreys, Effect of coalescence layer thickness on the properties of thin-chip InGaN/GaN light emitting diodes with embedded photonic quasi-crystal structures, Phys. Status Solidi 209 (2012) 451–455, http://dx.doi.org/10.1002/pssa.201100420.

[6] C.J. Lewins, E.D. Le Boulbar, S.M. Lis, P.R. Edwards, R.W. Martin, P.A. Shields, D.W.E. Allsopp, Strong photonic crystal behavior in regular arrays of core-shell and quantum disc InGaN/GaN nanorod light-emitting diodes, J. Appl. Phys. 116 (2014) 044305, http://dx.doi.org/10.1063/1.4891236.

[7] A. Yanagihara, S. Ishizawa, K. Kishino, Directional radiation beam from yellow-emitting InGaN-based nanocolumn LEDs with ordered bottom-up nanocolumn array, Appl. Phys. Express (1882) 112102, http://dx.doi.org/10.7567/APEX.7.112102.

[8] S. Krylyuk, D. Paramanik, M. King, A. Motayed, J.-Y. Ha, J.E. Bonevich, A. Talin, A. Davydov, Large-area GaN n-core/p-shell arrays fabricated using top-down etching and selective epitaxial overgrowth, Appl. Phys. Lett. 101 (2012) 241119, http://dx.doi.org/10.1063/1.4769376.

[9] A. De Luna Bugallo, L. Rigutti, G. Jacopin, F.H. Julien, C. Durand, X.J. Chen, D. Salomon, J. Eymery, M. Tchernycheva, Single-wire photodetectors based on InGaN/GaN radial quantum wells in GaN wires grown by catalyst-free metal-organic vapor phase epitaxy, Appl. Phys. Lett. 98 (2011) 233107, http://dx.doi.org/10.1063/1.3596446.

[10] G. Jacopin, L. Rigutti, S. Bellei, P. Lavenus, F.H. Julien, A.V. Davydov, D. Tsvetkov, K.A. Bertness, N.A. Sanford, J.B. Sclager, M. Tchernycheva, Photoluminescence polarization in strained GaN/AlGaN core/shell nanowires, Nanotechnology 23 (2012) 325701, http://dx.doi.org/10.1088/0957-4484/23/32/325701.

[11] M. Tchernycheva, A. Messanvi, A. de Luna Bugallo, G. Jacopin, P. Lavenus, L. Rigutti, H. Zhang, Y. Halioua, F.H. Julien, J. Eymery, C. Durand, Integrated photonic platform based on InGaN/GaN nanowire emitters and detectors, Nano Lett. 14 (2014) 3515–3520, http://dx.doi.org/10.1021/nl501124s.

[12] S.E.J. O'Kane, J. Sarma, D.W.E. Allsopp, A quasi-analytic modal expansion technique for modeling light emission from nanorod LEDs, IEEE J. Quantum Electron. 50 (2014) 774–781, http://dx.doi.org/10.1109/JQE.2014.2345024.

[13] T. Baba, Slow light in photonic crystals, Nat. Photonics 2 (2008) 465–473, http://dx.doi.org/10.1038/nphoton.2008.146.

[14] N. Niu, A. Woolf, D. Wang, T. Zhu, Q. Quan, R.A. Oliver, E.L. Hu, Ultra-low threshold gallium nitride photonic crystal nanobeam laser ultra-low threshold gallium nitride photonic crystal nanobeam laser, Appl. Phys. Lett. 106 (2015) 231104, http://dx.doi.org/10.1063/1.4922211.

[15] P.A. Shields, D.W.E. Allsopp, Nanoimprint lithography resist profile inversion for lift-off applications, Microelectron. Eng. 88 (2011) 3011–3014, http://dx.doi.org/10.1016/j.mee.2011.04.063.

[16] D. Paramanik, A. Motayed, G.S. Aluri, J.-Y. Ha, S. Krylyuk, A.V. Davydov, M. King, S. McLaughlin, S. Gupta, H. Cramer, Formation of large-area GaN nanostructures with controlled geometry and morphology using top-down fabrication scheme, J. Vac. Sci. Technol. B Microelectron. Nanometer Struct. 30 (2012) 052202, http://dx.doi.org/10.1116/1.4739424.

[17] E.D. Le Boulbar, I. Gîrgel, C.J. Lewins, P.R. Edwards, R.W. Martin, A. Šatka, D.W.E. Allsopp, P.A. Shields, Facet recovery and light emission from GaN/InGaN/GaN core-shell structures grown by metal organic vapour phase epitaxy on etched GaN nanorod arrays, J. Appl. Phys. 114 (2013) 094302, http://dx.doi.org/10.1063/1.4819440.

[18] J.-R. Chang, S.-P. Chang, Y.-J. Li, Y.-J. Cheng, K.-P. Sou, J.-K. Huang, H.-C. Kuo, C.-Y. Chang, Fabrication and luminescent properties of core-shell InGaN/GaN multiple quantum wells on GaN nanopillars, Appl. Phys. Lett. 100 (2012) 261103, http://dx.doi.org/10.1063/1.4731629.

[19] J.J. Wierer, Q. Li, D.D. Koleske, S.R. Lee, G.T. Wang, III-nitride core–shell nanowire arrayed solar cells, Nanotechnology 23 (2012) 194007, http://dx.doi.org/10.1088/0957-4484/23/19/194007.

[20] P. Shields, M. Hugues, J. Zúñiga-Pérez, M. Cooke, M. Dineen, W. Wang, F. Causa, D. Allsopp, Fabrication and properties of etched GaN nanorods, Phys. Status Solidi 9 (2012) 631–634, http://dx.doi.org/10.1002/pssc.201100394.

[21] S.J. Pearton, R.J. Shul, F. Ren, A review of dry etching of GaN and related materials, Internet journal nitride semiconductor research, MRS Internet J. Nitride Semicond. Res. 5 (2000) 1–38, http://dx.doi.org/10.1557/S1092578300000119.

[22] T. Senga, Y. Matsumi, M. Kawasaki, Chemical dry etching mechanism of GaAs surface by HCl and Cl_2, J. Vac. Sci. Technol. B 14 (1996) 3230, http://dx.doi.org/10.1116/1.588812.

[23] B. Rong, H.W.M. Salemink, E.M. Roeling, R. van der Heijden, F. Karouta, E. van der Drift, Fabrication of two dimensional GaN nanophotonic crystals (31), J. Vac. Sci. Technol. B Microelectron. Nanometer Struct. 25 (2007) 2632, http://dx.doi.org/10.1116/1.2794066.

[24] N. Okamoto, K. Imanishi, T. Kikkawa, N. Nara, Influence of Negative Charging on High Rate SiC Etching for GaN HEMT MMICs, Vols. 645-648Trans Tech Publ., 2010 791–794, http://dx.doi.org/10.4028/www.scientific.net/MSF.645-648.791.

[25] M. Schaepkens, G.S. Oehrlein, Asymmetric microtrenching during inductively coupled plasma oxide etching in the presence of a weak magnetic field, Appl. Phys. Express 72 (1998) 1293–1295, http://dx.doi.org/10.1063/1.121068.